ACS APPLIED MATERIALS & INTERFACES

Research Article

www.acsami.org

Designing 3D Highly Ordered Nanoporous CuO Electrodes for High-Performance Asymmetric Supercapacitors

Seyyed E. Moosavifard,[†] Maher F. El-Kady,[‡,#] Mohammad S. Rahmanifar,[§] Richard B. Kaner,*[,‡] and Mir F. Mousavi*[,†,‡]

[†]Department of Chemistry, Tarbiat Modares University, Tehran 14115-175, Iran

[‡]Department of Chemistry and Biochemistry and California Nanosystems Institute, University of California, Los Angeles (UCLA), Los Angeles, California 90095, United States

[#]Department of Chemistry, Faculty of Science, Cairo University, Giza 12613, Egypt

[§]Faculty of Basic Sciences, Shahed University, Tehran 18151-159, Iran

Web-Enhanced Feature *Supporting Information*

ABSTRACT: The increasing demand for energy has triggered tremendous research efforts for the development of light-weight and durable energy storage devices. Herein, we report a simple, yet effective, strategy for high-performance supercapacitors by building three-dimensional pseudocapacitive CuO frameworks with highly ordered and interconnected bimodal nanopores, nanosized walls (~4 nm) and large specific surface area of 149 $m^2 g^{-1}$. This interesting electrode structure plays a key role in providing facilitated ion transport, short ion and electron diffusion pathways and more active sites for electrochemical reactions. This electrode demonstrates excellent electrochemical performance with a specific capacitance of 431 F g^{-1} (1.51 F cm^{-2}) at 3.5 mA cm^{-2} and retains over 70% of this capacitance when operated at an ultrafast rate of 70 mA cm^{-2}. When this highly ordered CuO electrode is assembled in an asymmetric cell with an activated carbon electrode, the as-fabricated device demonstrates remarkable performance with an energy density of 19.7 W h kg^{-1}, power density of 7 kW kg^{-1}, and excellent cycle life. This work presents a new platform for high-performance asymmetric supercapacitors for the next generation of portable electronics and electric vehicles.

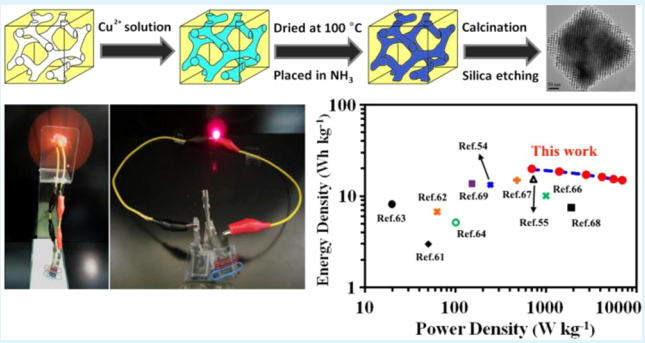

KEYWORDS: *3D highly ordered electrodes, nanoporous, copper oxide, asymmetric supercapacitor*

1. INTRODUCTION

Electrochemical capacitors, also known as supercapacitors (SCs) or ultracapacitors, are promising energy storage systems as they bridge the gap between traditional dielectric capacitors and chemical batteries. Supercapacitors are particularly useful in applications requiring fast charge/discharge rates such as power backup for electronic devices, cell phone cameras, regenerative braking and hybrid electric vehicles. Compared to batteries, supercapacitors exhibit significantly higher power density and long lifespan and are expected to have more industrial applications if their energy density can be improved.[1−4] This has driven the rapid growth of research in the field of supercapacitors. Much of these research efforts are directed toward the development of high performance and low cost electrode materials.[5,6] The selection of electrode materials for supercapacitors varies depending on the application and the way they store charge. SCs may store charge in one of the following mechanisms: (a) through electric double layer capacitance (EDLC) in carbonaceous materials and their hybrids (e.g., graphene, and graphene/carbon nanotubes),[7,8] and/or (b) by fast Faradaic redox reactions (pseudocapacitance) in conducting polymers and metal oxides. Due to the inherently low specific capacitance of carbonaceous materials, pseudocapacitors have attracted great interest.[6,9,10] Metal oxides often exhibit higher specific capacitances and electrochemical stability than most conductive polymers, so they are preferred as electrode materials for building high-energy supercapacitors.[11] Among these metal oxides, copper oxide (CuO) is a promising candidate due to its elemental abundance, non-toxicity, easy preparation in various shapes at the nanoscale and good electrochemical performance.[12] For example, Zhang et al.[13] reported flower-like nanostructured CuO that demonstrated a specific capacitance of 133.6 F g^{-1} in KOH electrolyte, while Li et al.[14] grew nanostructured CuO directly on copper foam with a specific capacitance of 212 F g^{-1} achieved in KOH electrolyte. Wang et al.[15] synthesized nanosheet arrays of CuO

Received: December 13, 2014
Accepted: February 11, 2015
Published: February 11, 2015

DOI: 10.1021/am508816t
ACS Appl. Mater. Interfaces 2015, 7, 4851−4860

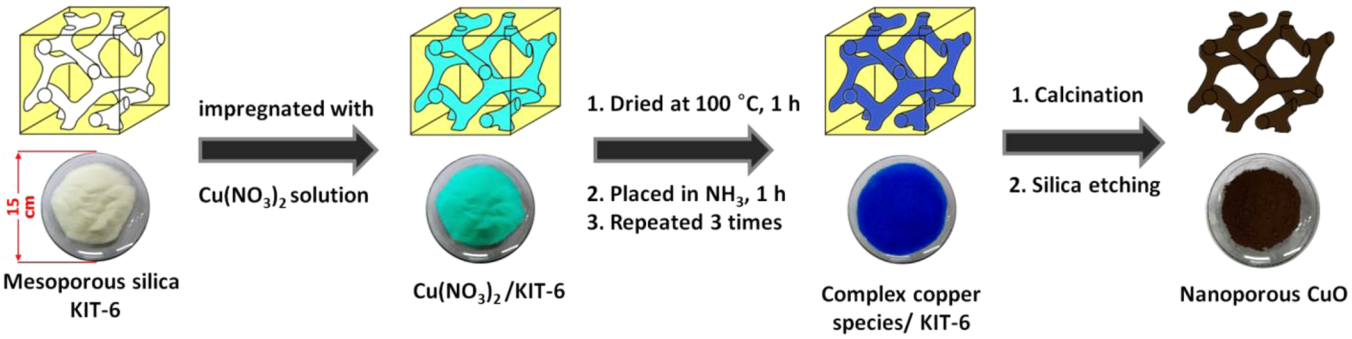

Figure 1. Schematic illustrations showing the synthesis of 3D highly ordered nanoporous CuO by nanocasting from KIT-6. Photos in the bottom show the size of the sample at each step of the synthesis and demonstrate a relatively scalable method.

on nickel foam with a high specific capacitance of 569 F g^{-1} in KOH electrolyte; however, the method employed is relatively complex and the yield is quite low. Recently, mesoporous CuO nanoribbons have been prepared in the presence of tetraoctylammonium bromide (TOAB) with a specific capacitance of 137 F g^{-1}.[16] 3D porous gear-like CuO has been reported on a Cu substrate with a specific capacitance of 348 F g^{-1}.[17]

Despite the notable progress in the preparation of CuO electrodes, low areal capacitances, low energy densities and slow rate capabilities remain challenging. The solution to these problems lies in improving the availability of active sites for pseudocapacitive reactions, accessibility of these sites to electrolyte, and providing short electron transport path ways for faster kinetics of the electrodes.[18−21] By using nanoporous silica as a template, it is possible to prepare pseudocapacitor electrodes with narrow particle size and pore size distributions, high surface area and large pore volume.[22−24] These structures can be designed to produce more active sites for charge storage reactions, more interconnected pores and better permeabilities.[25−28] Herein, we demonstrate, for the first time, the synthesis of 3D highly ordered nanoporous CuO electrodes with a bimodal pore size distribution, and high surface area, synthesized by nanocasting from KIT-6. This electrode exhibits high specific capacitance (431 F g^{-1} at 3.5 mA cm^{-2}), excellent rate capability and cycle life, unveiling its potential as a high-performance electrode material for supercapacitor application. In addition, an asymmetric supercapacitor based on nanoporous CuO as a positive electrode and activated carbon (AC) as a negative electrode demonstrates remarkable performance with an energy density of 19.7 W h kg^{-1}, power density of 7 kW kg^{-1} and excellent cycle life. We also utilized this asymmetric supercapacitor in practical applications in order to demonstrate the potential of this energy storage system as a power source for future electronics.

2. EXPERIMENTAL SECTION

2.1. Synthesis of 3D Highly Ordered Nanoporous CuO. Cubic *Ia3d* mesoporous silica KIT-6 was used as a hard template for the preparation of 3D highly ordered nanoporous CuO. This template was made as reported elsewhere.[29,30] In this process, tetraethyl orthosilicate (TEOS, Merck) was used as the silica source, while triblock copolymer Pluronic P123 (average MW = 5800, $EO_{20}PO_{70}EO_{20}$, Aldrich) was used as a structure-directing agent. In a typical synthesis, 10 g of P123 was dissolved in a mixture of concentrated HCl (16 mL, 37 wt %, Merck) and distilled water (360 mL) to form a homogeneous solution, to which 10 g of *n*-butanol (Merck) was added and stirred at 35 °C. After 1 h of stirring, 21.5 g of TEOS was added to the solution and kept under stirring for another 24 h. For the hydrothermal treatment and polymer cross-linking, the mixture was transferred to a Teflon-lined stainless steel autoclave and heated for 24 h at 50 °C. After the white solid product was filtered and dried, the polymer template (p123) was removed by extraction in a mixture of ethanol/HCl, followed by calcination in air at 550 °C for 3 h. This was followed by the preparation of nanoporous CuO using a nitrate combustion method.[31,32] As shown in Figure 1, in a typical synthesis, 4 g of KIT-6 was impregnated with 3 mL of an aqueous solution of $Cu(NO_3)_2{\cdot}3H_2O$ (1.5 g, Merck), followed by drying for 1 h at 100 °C. To allow for the formation of copper hydroxide in situ from copper ions without deimpregnation from the template, the copper precursor/silica composite was kept under ammonia vapor for 1 h at room temperature followed by drying. This process of impregnation-ammoniation-drying was repeated twice with an aqueous solution of 0.5 g $Cu(NO_3)_2{\cdot}3H_2O$. After drying, the resulting composite was heated slowly to 250 °C and calcined at this temperature for 4 h to obtain the CuO/silica nanostructure. Subsequently, to obtain nanoporous CuO, the resulting material was treated twice with a hot aqueous NaOH solution to remove the silica template, followed by washing with distilled water and absolute ethanol several times, and then dried at 60 °C. In order to synthesize bulk CuO, the above procedure was repeated without the silica template.

2.2. Materials Characterization. Prepared samples were characterized using X-ray powder diffraction (XRD, Philips X'pert diffractometer with Cu Kα radiation (λ = 0.154 nm) generated at 40 kV and 30 mA with a step size of 0.04° s^{-1}). TEM images were obtained on a transmission electron microscope (Philips EM 208, The Netherlands) equipped with an energy dispersive X-ray spectrometer (EDAX). Nitrogen adsorption/desorption measurements were performed using a Micromeritics ASAP-2010 apparatus at 77 K. Specific surface area was calculated from the multipoint Brunauer−Emmett−Teller (BET) method; and the pore size distribution was derived from the desorption branch of the nitrogen adsorption isotherm using the Barrett−Joyner−Halenda (BJH) method.

2.3. Electrochemical Measurements. The electrodes were made by mixing 80 wt % active material, 15 wt % carbon black, and 5 wt % polyvinylidenefluoride (PVDF) in *N*-methyl pyrrolidone (NMP). A 5% portion of solution was then mixed with acetone and sonicated for 30 min before it was spray coated onto a nickel foam current collector, and then dried at 120 °C for 2 h. The prepared electrode served as the working electrode in a three-electrode configuration, while a saturated calomel electrode (SCE) and a platinum plate were used as the reference and counter electrodes, respectively. All electrochemical measurements were performed in aqueous 3 M KOH solution at room temperature. Autolab PGSTAT30 was used for testing the electrochemical properties of the samples. A Solartron battery tester equipped with Cell Test software was used for galvanostatic charge/discharge (CD) investigations.

Electrode specific capacitance was derived through CD measurements using the following equation:

DOI: 10.1021/am508816t
ACS Appl. Mater. Interfaces 2015, 7, 4851−4860

$$C_{sp} = \frac{I\Delta t}{m\Delta V} \quad (1)$$

where C_{sp} is the specific capacitance, Δt is the discharge duration (s), I is the discharge current density (A), ΔV is the potential range (V), and m is the mass loading on the Ni foam (g).

2.4. Preparation of the Asymmetric Supercapacitor. The asymmetric supercapacitor was assembled based on the nanoporous CuO as the positive electrode and AC as the negative electrode with one piece of PE alkaline battery separator. Each electrode had a geometric surface area of 1 cm^2. To achieve the highest range of the working potential window, the mass ratio of the negative electrode to the positive electrode was determined according to the charge balance theory ($q^+ = q^-$). The voltammetric charges (Q) were calculated based on the following equations:

$$Q = C_{single} \times \Delta V \times m \quad (2)$$

where C_{single} is the specific capacitance (F g^{-1}) of each electrode measured in a three electrode setup (calculated from cyclic voltammograms at a scan rate of 10 mV s^{-1}), ΔV is the potential window (V), and m is the mass of the electrode (g). To maintain a charge balance between the two electrodes, the mass ratio between the positive (m_+) and negative (m_-) electrodes needs to follow:

$$\frac{m_+}{m_-} = \frac{C_- \times \Delta V_-}{C_+ \times \Delta V_+} \quad (3)$$

According to the specific capacitance values (177 F g^{-1} for AC and 390 F g^{-1} for nanoporous CuO) and the potential windows found for the AC and nanoporous CuO electrodes, the optimal mass ratio should be $m_+/m_- = 0.84$ in the asymmetric supercapacitors. Herein, the mass loadings of the negative and positive electrodes are 4.1 and 3.4 mg, respectively. So the total mass of the two active electrode materials is 7.5 mg cm^{-2}.

The energy density of the device was calculated from the discharge curves using the following equation:

$$ED = \frac{C_{sp}\Delta V^2}{2} \quad (4)$$

where C_{sp} is specific capacitance (F g^{-1}) and ΔV is the potential range (V); and power density was determined from the equation:

$$PD = \frac{ED}{\Delta t} \quad (5)$$

where ED is the energy density (W h kg^{-1}) and Δt is the discharge time.

3. RESULTS AND DISCUSSION

3.1. Characterization. The prepared samples were structurally characterized by low and wide-angle X-ray diffraction (XRD) analysis. Figure 2a shows wide-angle XRD patterns for the bulk and nanoporous CuO samples, confirming the crystallite phase purity of the as-prepared CuO. All diffraction peaks in the XRD patterns of the bulk and nanoporous samples can be readily indexed to the standard phase of monoclinic CuO (JCPDS card No. 05-0661, a = 4.684 Å, b = 3.425 Å, c = 5.129 Å, and β = 99.47°), with no characteristic peaks assigned to possible impurities such as $Cu(OH)_2$ or Cu_2O. Moreover, the broad diffraction peaks and low baseline of the nanoporous CuO sample verifies its nanocrystalline nature. Furthermore, no Si peaks were observed in the EDAX spectrum, confirming the complete removal of the silica template (Figure 2b). More information can be extracted from the low-angle XRD pattern for the 3D highly ordered nanoporous CuO, which is shown in the inset of Figure 2a. This pattern verifies the 3D mesostructure of CuO through the intense peak that appears at 2θ of 1−1.2° corresponding to the

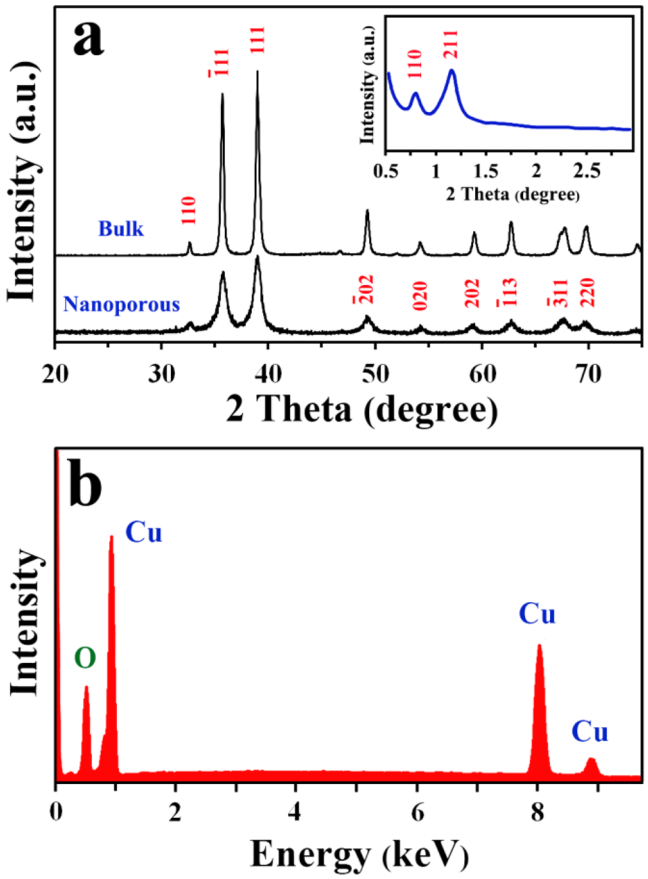

Figure 2. Spectroscopic characterization of bulk and nanoporous CuO samples. (a) Wide-angle XRD patterns of CuO samples. Inset is a low-angle XRD of the 3D highly ordered nanoporous CuO. (b) EDAX spectrum of the 3D highly ordered nanoporous CuO.

(211).[33,34] The other weak peak at a 2θ of 0.6−0.8° corresponds to the (110) diffraction peak and indicates the transformation of the cubic ($Ia3d$) mesostructure to a tetragonal ($I4_132$) or lower mesostructure.[35−37]

Transmission electron microscopy (TEM) further confirms the highly ordered nanostructure of the sample as shown in Figure 3a and b. One can see that the 3D mesoporous structure of the original silica template with nanosize wall thicknesses of about 4 nm is well preserved after the nanocasting replication. This morphology extends throughout the whole particle domain, which is in good agreement with XRD results. Moreover, no obvious nonporous particles are observed, indicating that almost all the metal nitrate was successfully filled inside the mesopores and then transformed in situ during the calcination. When CuO is prepared in the absence of KIT-6 template, the result is low surface area bulk and nonporous microparticles as shown in Figure 3c.

The corresponding nitrogen adsorption/desorption isotherm and BJH pore size distribution curve (inset) of the nanoporous CuO are shown in Figure 4. The isotherm of the as-synthesized CuO sample reflects a typical type IV sorption behavior with a hysteresis loop according to the IUPAC[38] classification, indicating a typical mesoporous structure which is consistent with TEM and low-angle XRD results. The BET specific surface area of this nanoporous CuO is calculated to be 149 m^2 g^{-1}. The BJH analysis (inset of Figure 4), reveals a bimodal pore size distribution centered at 4.9 and 10.8 nm. We can understand these results from the structure of KIT-6 that is

DOI: 10.1021/am508816t
ACS Appl. Mater. Interfaces 2015, 7, 4851−4860

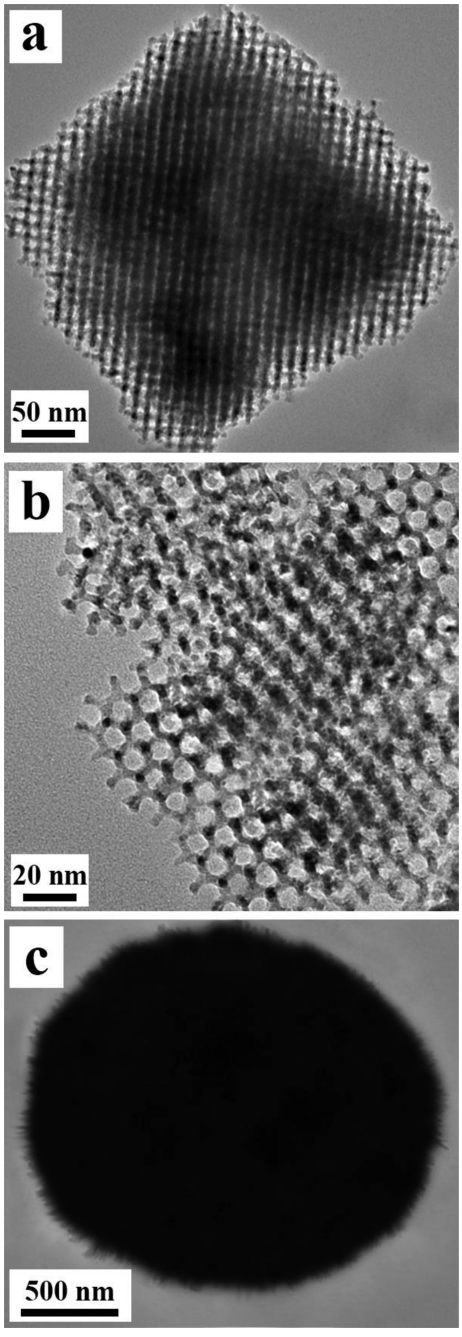

Figure 3. Microscopic characterization of bulk and nanoporous CuO. (a, b) Typical TEM images of the 3D highly ordered nanoporous CuO. (c) Typical TEM images of the bulk CuO.

known to have two sets of interpenetrating mesopores that are connected together through micropores in the walls of the template (see Scheme S1 in the Supporting Information). The bimodal structure of nanoporous CuO means that in some parts of the template CuO grows in both channels of the interpenetrating mesopores, whereas in other regions CuO grows in only one set of mesopores.[39−41] TEM images support this conclusion as well. We observe coupled mesoporous structure in the central regions of the template that results when CuO is replicated from both channels of KIT-6, whereas uncoupled mesopores can be seen in the edges in which CuO is filling only one channel as shown in Supporting Information Scheme S1. This 3D highly ordered nanoporous structure with

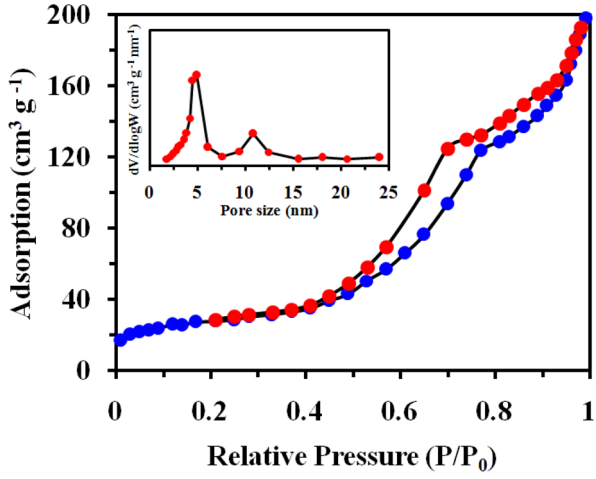

Figure 4. N_2 adsorption−desorption isotherms and corresponding BJH pore size distribution curve for the 3D highly ordered nanoporous CuO.

nanocrystalline walls, high surface area and conjunct bimodal pores can play key roles in providing shorter diffusion paths and rapid electrolyte transport, while providing more active sites for electrochemical reactions.[18,22,32,42]

3.2. Electrochemical Evaluation. To evaluate the electrochemical properties of the nanoporous CuO, cyclic voltammetry (CV) and galvanostatic charge−discharge (CD) measurements were conducted in a three-electrode cell. Figure 5a shows typical CVs of the bare Ni foam (current collector), and bulk and nanoporous CuO electrodes in 3 M KOH aqueous electrolyte at a scan rate of 5 mV s^{-1}. In a control experiment, we found that the current produced by the nickel foam is quite low when compared to CuO, meaning that the current collector does not contribute to the capacitance. Remarkably, the current signal generated by the nanoporous CuO electrode is much larger than that of the bulk sample, indicating a significant increase in the specific capacitance. The strong pair of anodic and cathodic peaks within 0.1−0.4 V can be attributed to the Faradaic redox reactions of the Cu(I)/Cu(II) transition (as described in Supporting Information), clearly showing that the charge storage mechanism of the CuO electrodes is through pseudocapacitance.[15,43,44] Figure 5b shows typical CV curves of the nanoporous CuO electrode in aqueous 3 M KOH electrolyte at various scan rates. We observe that the CV curves remained almost unchanged by increasing the scan rate, which confirms the improved mass transport, excellent reversibility and high rate capability of the electrode.[45]

The electrochemical performance of the new material in supercapacitors was further investigated at constant current densities using charge−discharge measurements. Figure 5c and d show the CD curves of the 3D nanoporous CuO electrode in 3 M KOH solution at increasing current densities from 3.5 to 175 mA cm^{-2} (1 to 50 A g^{-1}) in the potential range of −0.1−0.4 V (vs SCE). Clearly, the nonlinear behavior of the CD curves further verifies the result from the CV measurements that the main sources for charge storage in the nanoporous CuO electrodes originate from Faradaic reactions. Furthermore, the charge curves indicate that most of the capacitance is generated in the potential range of 0.1−0.4 V, corresponding to the Faradaic redox reactions of the Cu^{+}/Cu^{2+} transition which is in good agreement with the CV results. Nanoporous CuO demonstrates an ultrahigh specific capacitance of 431 F g^{-1}

DOI: 10.1021/am508816t
ACS Appl. Mater. Interfaces 2015, 7, 4851−4860

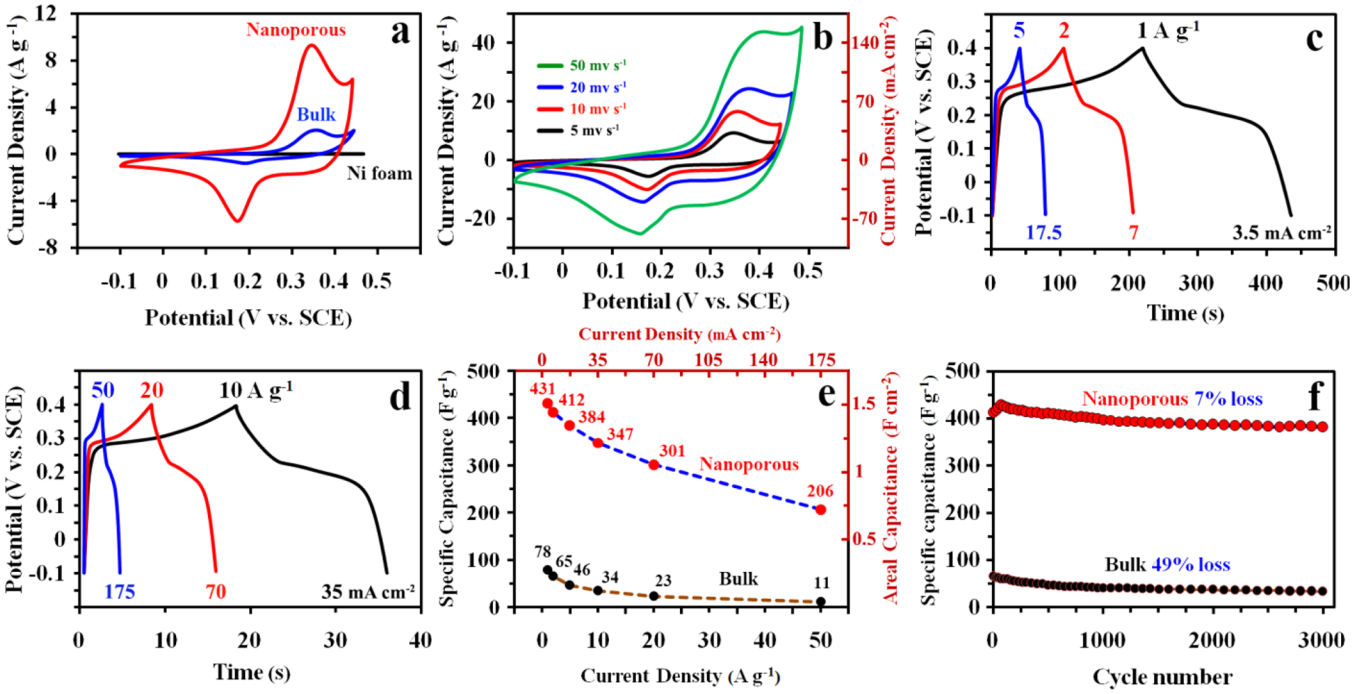

Figure 5. Evaluation of the electrochemical performance of CuO electrodes in a three-electrode system. (a) CV of the current collector (bare Ni foam) and the as-prepared CuO electrodes in aqueous 3 M KOH electrolyte at a scan rate of 5 mV s^{-1}, (b) CV curves of the 3D highly ordered nanoporous CuO electrode at various scan rates (c, d) galvanostatic charge−discharge curves of the nanoporous CuO electrode at various current densities, (e) rate capability of the CuO electrodes, and (f) long-term cycling stability of the CuO electrodes at current density of 7 mA cm^{-2}.

(1.51 F cm^{-2}) at 3.5 mA cm^{-2}, a value that is substantially higher than bulk CuO (78 F g^{-1}) and previously reported CuO materials (see Supporting Information Table S1). Not only does nanoporous CuO show high specific capacitance, but it also maintains its excellent electrochemical performance even when operated at high charge/discharge rates. For example, Figure 5e illustrates the dependence of the specific gravimetric and areal capacitances as a function of the applied current densities for bulk and nanoporous CuO electrodes. The specific capacitance of the nanoporous CuO electrode at 70 (20 A g^{-1}) and 175 mA cm^{-2} (50 A g^{-1}) is as much as 70% and 48% of that at 3.5 mA cm^{-2} (1 A g^{-1}). These results clearly demonstrate the excellent rate capability of the nanoporous CuO electrode under high current densities, which is important for practical supercapacitor applications.

The long-term cycling stability of the CuO electrodes was also investigated by continuous CD measurements over 3000 cycles at a current density of 7 mA cm^{-2} within a voltage range of −0.1−0.4 V as shown in Figure 5f. The specific capacitance of nanoporous electrode slightly increased during the initial cycles, which can be attributed to an activation process that enables trapped cations in the CuO crystal lattice to gradually diffuse out;[16,46] by cycle 3000 the specific capacitance has gradually decreased to 383 F g^{-1} corresponding to a capacitance loss of 7%, which is substantially lower than bulk CuO (49%) and indicates remarkable long-term cycling stability of the nanoporous electrode. In addition, a comparison of the electrochemical performance of 3D highly ordered nanoporous CuO with previously reported CuO materials is presented in Supporting Information Table S1. The large capacitance, excellent rate capability, and remarkable long-term cycling stability of the nanoporous CuO electrode can be attributed to the following unique structural features: first, a 3D highly ordered structure with interconnected narrow and wide nanopores (4.9 and 10.8 nm) which enhances the accessibility of electrolyte in conjunct nanopores by acting as ion-buffering reservoirs thus minimizing the diffusion distance from the external electrolyte to the interior surfaces;[9,22,23] second, the high specific surface area (149 m^2 g^{-1}) which improves the utilization of the active material by providing more active sites for the electrochemical reactions;[42,45] and third, the nanosized walls (∼4 nm) which lead to higher conductivity and faster kinetics by providing short diffusion/transport pathways for both electrons and ions.[18,47,48]

The electrochemical impedance spectroscopy (EIS) further supports the excellent electrochemical behavior of nanoporous CuO electrodes; the Nyquist plots are shown in Figure 6. Both electrodes reveal a semicircle at high frequencies followed by a linear slope at the medium or low frequency region. The depressed semicircle at the high frequency region corresponds to charge transfer resistance (R_{ct}) caused by Faradaic reactions,[49,50] which can be attributed to the Cu^{2+}/Cu^{+} redox couple. The straight line in the medium frequency region can be ascribed to Warburg impedance[51] related to the diffusion of electrolyte within the CuO structure. The steeper line at low frequencies demonstrates the capacitive nature of the electrode (vertical line for an ideal capacitor). Accordingly, the nanoporous CuO electrode exhibits a low charge transfer resistance (R_{ct}) and low internal resistance (R_b), suggesting a higher electrical conductivity, and a larger electro-active surface area for the electrode.[23] In addition, the plot shows a more vertical line for the nanoporous CuO in the low frequency region, indicating that the interconnected porous channels of the CuO electrode facilitate the mass transfer of the electrolyte.[52,53] Furthermore, EIS plots of the nanoporous CuO electrode before and after cycling indicate that both impedance spectra are nearly identical, further confirming the excellent cycling stability. All of these results demonstrate the

DOI: 10.1021/am508816t
ACS Appl. Mater. Interfaces 2015, 7, 4851−4860

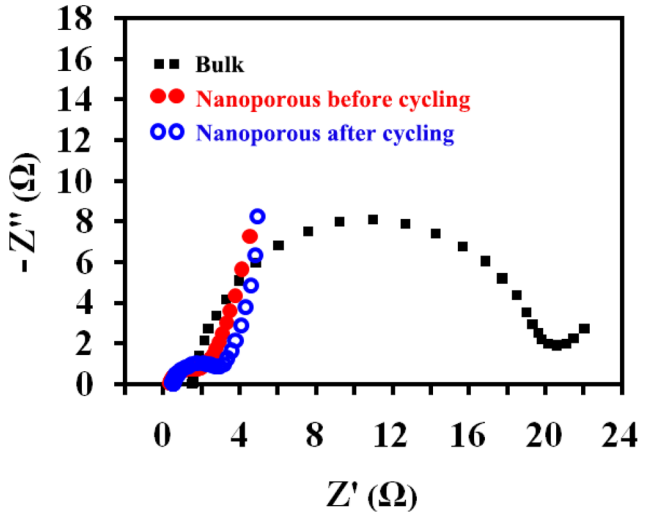

Figure 6. Electrochemical impedance spectroscopy (EIS) plot of the bulk and nanoporous CuO electrode before and after cycling.

desirable pseudocapacitance characteristic features of nanoporous CuO making it a promising electrode material for supercapacitor applications.

3.3. Building Asymmetric Supercapacitors. The energy density and power density of an aqueous supercapacitor can be significantly improved by employing an asymmetric configuration. In this design, the active material in one electrode is different from that used in the other. This extends the operating voltage of the cell beyond the thermodynamic decomposition voltage of water, that is, >1.2 V. We assembled an asymmetric supercapacitor using activated carbon (AC) as the negative electrode and the 3D nanoporous CuO as the positive electrode. The CV curves for AC and nanoporous CuO electrodes at a scan rate of 10 mV s^{-1} in 3 M KOH aqueous solution are shown in Figure 7a. As can be seen, the potential windows of the AC and nanoporous CuO electrodes are −1.0−0 and −0.1−0.44 V, respectively. The AC electrode has a nearly rectangular CV curve, limited by H_2 evolution, indicating a typical EDLC behavior since no redox peaks are observed. On the other hand, the CV shape of the nanoporous CuO displays pseudocapacitance behavior, limited by O_2 evolution, based on a redox mechanism. The total cell voltage can be expressed as the sum of the potential range for the AC and the nanoporous CuO electrodes. Therefore, the cell potential can be as high as 1.4 V in 3 M aqueous KOH electrolyte, which is higher than that of conventional AC-based symmetric supercapacitors in aqueous electrolytes (0.8−1.0 V). Figure 7b and c shows the CV and CD of nanoporous CuO//AC at different voltage windows in 3 M KOH electrolyte at 20 mV s^{-1} and 7.5 mA cm^{-2}, respectively. As can be seen, the potential windows of the asymmetric supercapacitor can be extended to 1.4 V, and its CV and CD curves reveal the contributions of both EDLC and pseudocapacitance. When the working potential window is 0.0−0.4 and 0.0−0.7 V, only the EDLC mechanism is operative. By increasing the working potential windows, the redox peaks appear, and the behavior of the asymmetric supercapacitor deviates from the ideal rectangular shape owing to Faradaic redox reactions. Figure 7d shows the typical CV curves of the nanoporous CuO//AC asymmetric supercapacitor at various scan rates from 5 to 50 mV s^{-1}. The shape of the CV curves is not significantly influenced by an increasing scan rate, indicating high rate capability and good reversibility of the supercapacitor. Figure 7e shows the CD curves of the nanoporous CuO//AC asymmetric supercapacitor at different current densities from 7.5 to 75 mA cm^{-2} (1 to 10 A g^{-1}) with a voltage window of 0−1.4 V. As shown, at a cell voltage as high as 1.4 V, both charge and

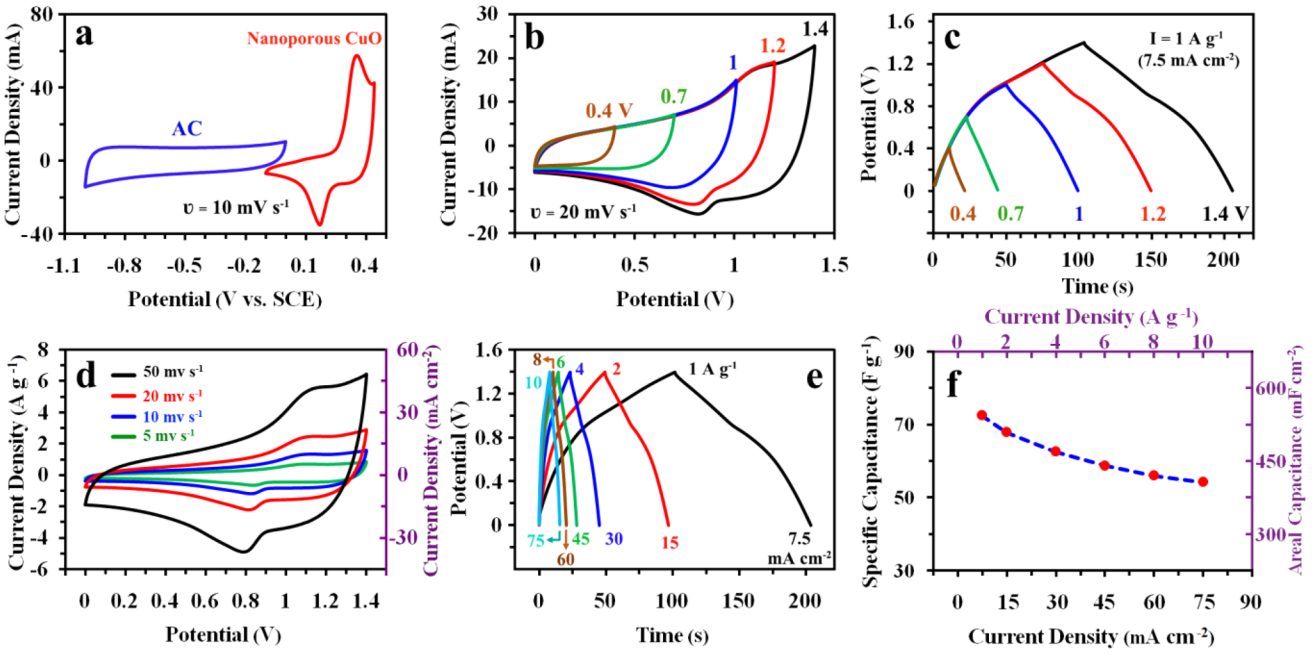

Figure 7. Electrochemical performance of a nanoporous CuO//AC asymmetric supercapacitor. (a) CV curves of 3D highly ordered nanoporous CuO and AC electrodes at a scan rate of 10 mV s^{-1} in a three-electrode system, (b) CVs of the nanoporous CuO//AC asymmetric supercapacitor at different potential windows at 20 mV s^{-1}, (c) CD curves of the asymmetric supercapacitor at different potential windows at a fixed current density of 7.5 mA cm^{-2}, (d) CVs at different scan rates, (e) CD curves at different current densities, and (f) the rate capability of the asymmetric supercapacitor.

DOI: 10.1021/am508816t
ACS Appl. Mater. Interfaces 2015, 7, 4851−4860

discharge curves maintain very good symmetry indicating the excellent capacitance characteristics and electrochemical reversibility. Figure 7f shows the values of the mass and areal specific capacitances at various current densities based on the corresponding discharge curves. The gravimetric and areal specific capacitance values are 72.4, 67.8, 62.5, 58.7, 56, and 54.2 F g^{-1} (543, 508, 469, 440, 420, and 406 mF cm^{-2}) at current densities of 1, 2, 4, 6, 8, and 10 A g^{-1} (7.5, 15, 30, 45, 60, and 75 mA cm^{-2}), respectively. A maximum capacitance value of 72.4 F g^{-1} (0.543 F cm^{-2}) at 1 A g^{-1} (7.5 mA cm^{-2}) was achieved, which is higher than that of other asymmetric supercapacitors previously reported including Co_3O_4 NSs–rGO//AC (46 F g^{-1}),[54] $NiCo_2O_4$ NSs@HMRAs//AC (49.3 F g^{-1}),[55] NiO//rGO (50 F g^{-1}),[56] Ni_3S_2/CNFs//CNFs (56.6 F g^{-1})[57] and α-$Co(OH)_2/Co_3O_4$//AC (71 F g^{-1}).[58] To the best of our knowledge, this is the first example of an asymmetric supercapacitor using CuO as a positive electrode.

Another interesting advantage of the asymmetric configuration is that it combines Faradaic and non-Faradaic processes by coupling an EDLC electrode with a pseudocapacitor electrode, which may boost the cycling stability of the whole cell. This was tested by carrying out continuous CD measurements at a current density of 15 mA cm^{-2} within the voltage range of 0–1.4 V as shown in Figure 8a. There is only a 4% capacity loss after 3000 cycles, indicating excellent cycling stability of nanoporous CuO//AC asymmetric supercapacitor.

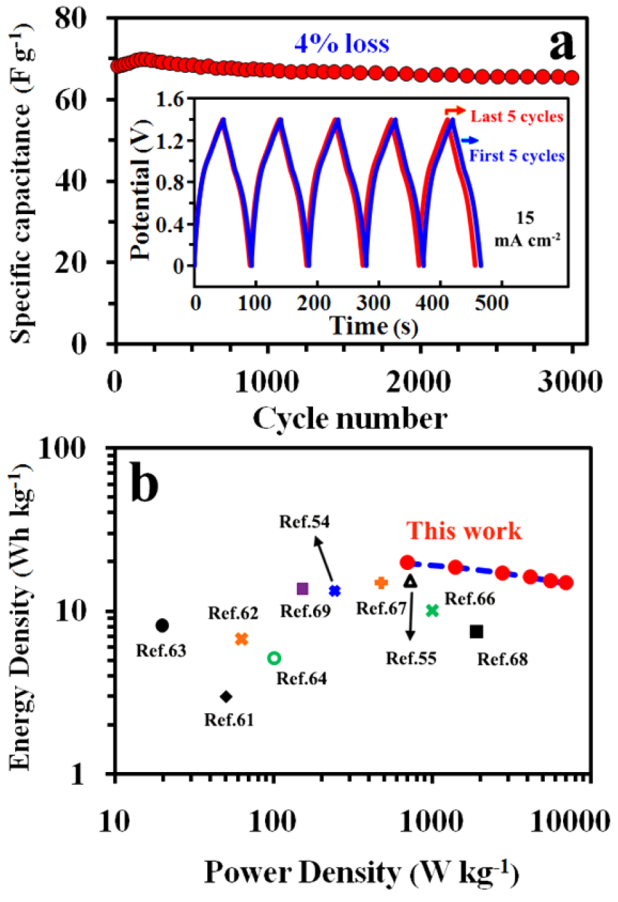

Figure 8. (a) Long-term cycling stability of the nanoporous CuO//AC asymmetric supercapacitor at a current density of 15 mA cm^{-2}. (b) Ragone plot of the asymmetric supercapacitor compared with other reported data.

Power density (PD) and energy density (ED) are considered the two most important parameters of a supercapacitor device which determine its operational performance/efficiency.[59,60] In order to demonstrate the overall performance of the nanoporous CuO//AC asymmetric supercapacitor, a Ragone plot showing the energy density and power density at various current densities is presented in Figure 8b. Also, for comparison, the data for a few typical examples previously reported are provided. A maximum energy density of 19.7 W h kg^{-1} was achieved by the asymmetric supercapacitor at a power density of 700 W kg^{-1}. The obtained energy density is higher than that of symmetrical supercapacitors such as rGO//rGO (<4 W h kg^{-1}),[61] 3D graphene/MnO_2//3D graphene/MnO_2 (6.8 W h kg^{-1}),[62] graphene/MnO_2//graphene/MnO_2 (8.1 W h kg^{-1}),[63] CNTs//CNTs (<10 W h kg^{-1}),[64] and AC//AC supercapacitors (<10 W h kg^{-1}).[27,58,65] It is also higher than that of previously reported asymmetric supercapacitors such as NiO//carbon (10 W h kg^{-1}),[66] GHCS-MnO_2//GHCS (15 W h kg^{-1}),[67] Ni–Co oxide//AC (7.4 W h kg^{-1}),[68] $Co(OH)_2$-nanowires//AC (13.6 W h kg^{-1}),[69] Co_3O_4 NSs-rGO//AC (13.4 W h kg^{-1}),[54] $NiCo_2O_4$ NSs@HMRAs//AC (15.42 W h kg^{-1}),[55] Co_3O_4@MnO_2//MEGO (17.7 W h kg^{-1}).[70] Figure 9 show two examples that demonstrate the potential of a CuO//AC asymmetric supercapacitor for practical applications. Strikingly, as shown in Figure 9a and Video 1, a single cell

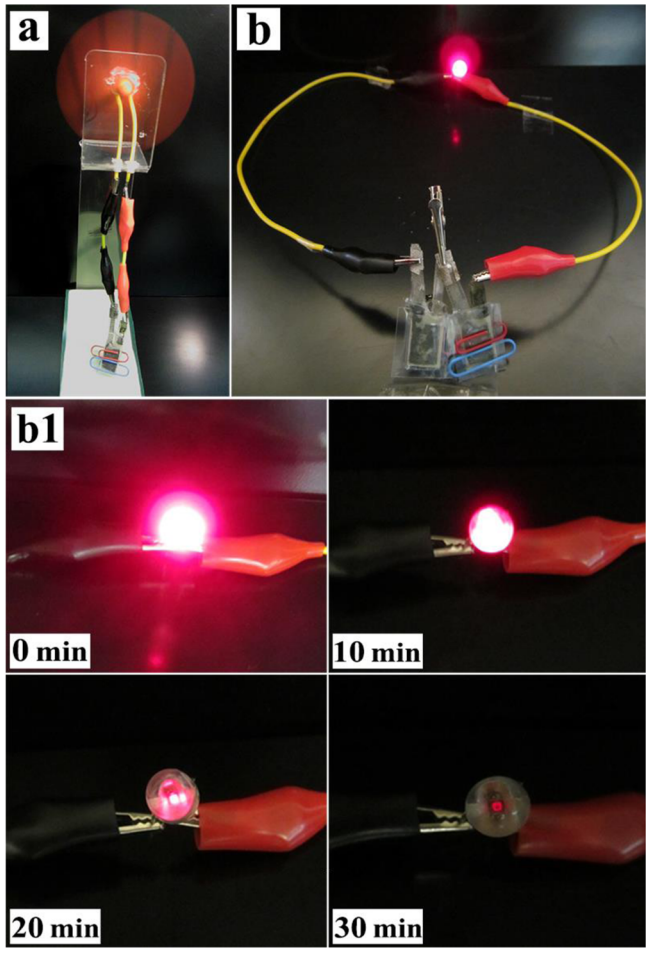

Figure 9. (a) Picture showing that one prepared device can drive a rotating motor. (b) Red LED lit up by two prepared devices in series and (b1) images of the red LED at different stages (b1).

DOI: 10.1021/am508816t
ACS Appl. Mater. Interfaces 2015, 7, 4851–4860

can drive a mini-motor (1.3 V, 30 mW) rotating robustly for approximately 160 s after charging for only 30 s to ~1.4 V. Furthermore, when using two cells connected in series, as shown in Figure 9b and Video 2, a red (8 mm, 20 mA) light-emitting diode (LED) was lit up for more than 30 min. These attractive results make the 3D highly ordered nanoporous CuO a promising electrode material for high-performance energy storage systems.

4. CONCLUSIONS

We have developed 3D highly ordered CuO electrodes with interconnected bimodal nanopores, high specific surface area, and nanosized walls. This unique structure allows the efficient use of the pseudocapacitive properties of CuO for charge storage, enabling the fabrication of CuO//AC asymmetric supercapacitors with excellent electrochemical performance including high specific capacitance, high rate capability, long cycle life and high energy density. This remarkable performance contrasts with CuO made by traditional methods, giving some insights into the design of high-performance metal oxide electrodes for supercapacitor applications. We envision these 3D CuO electrodes to be useful in a broad range of applications such as supercapacitors, lithium ion batteries, fuel cells, gas sensors, biosensors, catalysis, and other electronic devices.

■ ASSOCIATED CONTENT

Ⓢ Supporting Information

Redox reactions describing the charge storage mechanism of CuO in alkaline media, schematic illustration of the bimodal pore size distribution and a table comparing electrochemical performance of 3D nanoporous CuO prepared in this work and of other CuO materials reported in previous work. This material is available free of charge via the Internet at http://pubs.acs.org.

Ⓦ Web-Enhanced Features

Videos showing a single cell can drive a mini-motor and two cells connected in series are available in the HTML version of the paper.

■ AUTHOR INFORMATION

Corresponding Authors

*E-mail: kaner@chem.ucla.edu.
*E-mail: mousavi@chem.ucla.edu.

Notes

The authors declare no competing financial interest.

■ ACKNOWLEDGMENTS

This work was made possible through Tarbiat Modares University Research Council, and Nanotech Energy, Inc. (R.B.K.).

■ REFERENCES

(1) Wang, G.; Zhang, L.; Zhang, J. A Review of Electrode Materials for Electrochemical Supercapacitors. *Chem. Soc. Rev.* **2012**, *41*, 797–828.
(2) Simon, P.; Gogotsi, Y. Materials for Electrochemical Capacitors. *Nat. Mater.* **2008**, *7*, 845–854.
(3) Liu, C.; Li, F.; Ma, L. P.; Cheng, H. M. Advanced Materials for Energy Storage. *Adv. Mater.* **2010**, *22*, E28–E62.
(4) Butt, F. K.; Tahir, M.; Cao, C.; Idrees, F.; Ahmed, R.; Khan, W. S.; Ali, Z.; Mahmood, N.; Tanveer, M.; Mahmood, A.; Aslam, I. Synthesis of Novel ZnV_2O_4 Hierarchical Nanospheres and Their Applications as Electrochemical Supercapacitor and Hydrogen Storage Material. *ACS Appl. Mater. Interfaces* **2014**, *6*, 13635–13641.
(5) Gao, W.; Singh, N.; Song, L.; Liu, Z.; Reddy, A. L. M.; Ci, L.; Vajtai, R.; Zhang, Q.; Wei, B.; Ajayan, P. M. Direct Laser Writing of Micro-Supercapacitors on Hydrated Graphite Oxide Films. *Nat. Nanotechnol.* **2011**, *6*, 496–500.
(6) Wei, T. Y.; Chen, C. H.; Chien, H. C.; Lu, S. Y.; Hu, C. C. A Cost-Effective Supercapacitor Material of Ultrahigh Specific Capacitances: Spinel Nickel Cobaltite Aerogels from an Epoxide-Driven Sol–Gel Process. *Adv. Mater.* **2010**, *22*, 347–351.
(7) Dai, L.; Chang, D. W.; Baek, J. B.; Lu, W. Carbon Nanomaterials for Advanced Energy Conversion and Storage. *Small* **2012**, *8*, 1130–1166.
(8) Liu, J.; Zhang, L.; Wu, H. B.; Lin, J.; Shen, Z.; Lou, X. W. High-Performance Flexible Asymmetric Supercapacitors Based on a New Graphene Foam/Carbon Nanotube Hybrid Film. *Energy Environ. Sci.* **2014**, *7*, 3709–3719.
(9) Meher, S. K.; Rao, G. R. Ultralayered Co_3O_4 for High-Performance Supercapacitor Applications. *J. Phys. Chem. C* **2011**, *115*, 15646–15654.
(10) Liang, K.; Tang, X.; Hu, W. High-Performance Three-Dimensional Nanoporous NiO Film as a Supercapacitor Electrode. *J. Mater. Chem. A* **2012**, *22*, 11062–11067.
(11) Hulicova-Jurcakova, D.; Kodama, M.; Shiraishi, S.; Hatori, H.; Zhu, Z. H.; Lu, G. Q. Nitrogen-Enriched Nonporous Carbon Electrodes with Extraordinary Supercapacitance. *Adv. Funct. Mater.* **2009**, *19*, 1800–1809.
(12) Pendashteh, A.; Mousavi, M. F.; Rahmanifar, M. S. Fabrication of Anchored Copper Oxide Nanoparticles on Graphene Oxide Nanosheets via an Electrostatic Coprecipitation and its Application as Supercapacitor. *Electrochim. Acta* **2013**, *88*, 347–357.
(13) Zhang, H.; Feng, J.; Zhang, M. Preparation of Flower-Like CuO by a Simple Chemical Precipitation Method and Their Application as Electrode Materials for Capacitor. *Mater. Res. Bull.* **2008**, *43*, 3221–3226.
(14) Li, Y.; Chang, S.; Liu, X.; Huang, J.; Yin, J.; Wang, G.; Cao, D. Nanostructured CuO Directly Grown on Copper Foam and Their Supercapacitance Performance. *Electrochim. Acta* **2012**, *85*, 393–398.
(15) Wang, G.; Huang, J.; Chen, S.; Gao, Y.; Cao, D. Preparation and Supercapacitance of CuO Nanosheet Arrays Grown on Nickel Foam. *J. Power Sources* **2011**, *196*, 5756–5760.
(16) Zhang, Y. X.; Huang, M.; Kuang, M.; Liu, C. P.; Tan, J. L.; Dong, M.; Yuan, Y.; Zhao, X. L.; Wen, Z. Facile Synthesis of Mesoporous CuO Nanoribbons for Electrochemical Capacitors Applications. *Int. J. Electrochem. Sci.* **2013**, *8*, 1366–1381.
(17) Yu, L.; Jin, Y.; Li, L.; Ma, J.; Wang, G.; Geng, B.; Zhang, X. 3D Porous Gear-Like Copper Oxide and Their High Electrochemical Performance as Supercapacitors. *CrystEngComm.* **2013**, *15*, 7657–7662.
(18) Pinkert, K.; Giebeler, L.; Herklotz, M.; Oswald, S.; Thomas, J.; Meier, A.; Borchardt, L.; Kaskel, S.; Ehrenberg, H.; Eckert, J. Functionalised Porous Nanocomposites: a Multidisciplinary Approach to Investigate Designed Structures for Supercapacitor Applications. *J. Mater. Chem. A* **2013**, *1*, 4904–4910.
(19) Deng, M. J.; Wang, C. C.; Ho, P. J.; Lin, C. M.; Chen, J. M.; Lu, K. T. Facile Electrochemical Synthesis of 3D Nano-Architectured CuO Electrodes for High-Performance Supercapacitors. *J. Mater. Chem. A* **2014**, *2*, 12857–12865.
(20) Lu, Q.; Chen, Y.; Li, W.; Chen, J.; Xiao, J. Q.; Jiao, F. Ordered Mesoporous Nickel Cobaltite Spinel with Ultra-High Supercapacitance. *J. Mater. Chem. A* **2013**, *1*, 2331–2336.
(21) Cai, D.; Wang, D.; Liu, B.; Wang, L.; Liu, Y.; Li, H.; Wang, Y.; Li, Q.; Wang, T. Three-Dimensional Co_3O_4@$NiMoO_4$ Core/Shell Nanowire Arrays on Ni Foam for Electrochemical Energy Storage. *ACS Appl. Mater. Interfaces* **2014**, *6*, 5050–5055.
(22) Ye, Y.; Jo, C.; Jeong, I.; Lee, J. Functional Mesoporous Materials for Energy Applications: Solar Cells, Fuel Cells, and Batteries. *Nanoscale* **2013**, *5*, 4584–4605.

DOI: 10.1021/am508816t
ACS Appl. Mater. Interfaces 2015, 7, 4851–4860

(23) Cai, D.; Liu, B.; Wang, D.; Liu, Y.; Wang, L.; Li, H.; Wang, Y.; Wang, C.; Li, Q.; Wang, T. Enhanced Performance of Supercapacitors with Ultrathin Mesoporous $NiMoO_4$ Nanosheets. *Electrochim. Acta* **2014**, *125*, 294−301.
(24) Wang, G.; Liu, H.; Horvat, J.; Wang, B.; Qiao, S.; Park, J.; Ahn, H. Highly Ordered Mesoporous Cobalt Oxide Nanostructures: Synthesis, Characterisation, Magnetic Properties, and Applications for Electrochemical Energy Devices. *Chem.—Eur. J.* **2010**, *16*, 11020−11027.
(25) Xu, K.; Zou, R.; Li, W.; Liu, Q.; Liu, X.; An, L.; Hu, J. Design and Synthesis of 3D Interconnected Mesoporous $NiCo_2O_4$@$Co_xNi_{1-x}(OH)_2$ Core-Shell Nanosheet Arrays with Large Areal Capacitance and High Rate Performance for Supercapacitors. *J. Mater. Chem. A* **2014**, *2*, 10090−10097.
(26) Liu, D.; Yang, Z.; Wang, P.; Li, F.; Wang, D.; He, D. Preparation of 3D Nanoporous Copper-Supported Cuprous Oxide for High-Performance Lithium Ion Battery Anodes. *Nanoscale* **2013**, *5*, 1917−1921.
(27) Ma, X. J.; Kong, L. B.; Zhang, W. B.; Liu, M. C.; Luo, Y. C.; Kang, L. Design and Synthesis of 3D Co_3O_4@$MMoO_4$ (M = Ni, Co) Nanocomposites as High-Performance Supercapacitor Electrodes. *Electrochim. Acta* **2014**, *130*, 660−669.
(28) Lei, Y.; Li, J.; Wang, Y.; Gu, L.; Chang, Y.; Yuan, H.; Xiao, D. Rapid Microwave-Assisted Green Synthesis of 3D Hierarchical Flower-Shaped $NiCo_2O_4$ Microsphere for High-Performance Supercapacitor. *ACS Appl. Mater. Interfaces* **2014**, *6*, 1773−1780.
(29) Kleitz, F.; Hei Choi, S.; Ryoo, R. Cubic *Ia*3*d* Large Mesoporous Silica: Synthesis and Replication to Platinum Nanowires, Carbon Nanorods and Carbon Nanotubes. *Chem. Commun.* **2003**, *0*, 2136−2137.
(30) Kim, T. W.; Kleitz, F.; Paul, B.; Ryoo, R. MCM-48-like Large Mesoporous Silicas with Tailored Pore Structure: Facile Synthesis Domain in a Ternary Triblock Copolymer−Butanol−Water System. *J. Am. Chem. Soc.* **2005**, *127*, 7601−7610.
(31) Ren, Y.; Ma, Z.; Qian, L.; Dai, S.; He, H.; Bruce, P. Ordered Crystalline Mesoporous Oxides as Catalysts for CO Oxidation. *Catal. Lett.* **2009**, *131*, 146−154.
(32) Ren, Y.; Ma, Z.; Bruce, P. G. Ordered Mesoporous Metal Oxides: Synthesis and Applications. *Chem. Soc. Rev.* **2012**, *41*, 4909−4927.
(33) Solovyov, L. A.; Zaikovskii, V. I.; Shmakov, A. N.; Belousov, O. V.; Ryoo, R. Framework Characterization of Mesostructured Carbon CMK-1 by X-ray Powder Diffraction and Electron Microscopy. *J. Phys. Chem. B* **2002**, *106*, 12198−12202.
(34) Rumplecker, A.; Kleitz, F.; Salabas, E.-L.; Schüth, F. Hard Templating Pathways for the Synthesis of Nanostructured Porous Co_3O_4. *Chem. Mater.* **2007**, *19*, 485−496.
(35) Shon, J. K.; Kong, S. S.; Kim, J. M.; Ko, C. H.; Jin, M.; Lee, Y. Y.; Hwang, S. H.; Yoon, J. A.; Kim, J.-N. Facile Synthesis of Highly Ordered Mesoporous Silver Using Cubic Mesoporous Silica Template with Controlled Surface Hydrophobicity. *Chem. Commun.* **2009**, *0*, 650−652.
(36) Jin, M.; Park, J. N.; Shon, J.; Li, Z.; Lee, E.; Kim, J. Highly Ordered Crystalline Mesoporous Metal Oxides for Hydrogen Peroxide Decomposition. *J. Porous Mater.* **2013**, *20*, 7657−7662.
(37) Solovyov, L. A. Diffraction Analysis of Mesostructured Mesoporous Materials. *Chem. Soc. Rev.* **2013**, *42*, 3708−3720.
(38) Sing, K. S. W.; Everett, D. H.; Haul, R. A. W.; Moscou, L.; Pierotti, R. A.; Rouquerol, J.; Siemieniewska, T. Reporting Physisorption Data for Gas/Solid Systems with Special Reference to the Determination of Surface Area and Porosity (Recommendations 1984). *Pure Appl. Chem.* **1985**, *57*, 603−619.
(39) Tüysüz, H.; Weidenthaler, C.; Grewe, T.; Salabaş, E. L.; Benitez Romero, M. J.; Schüth, F. A Crystal Structure Analysis and Magnetic Investigation on Highly Ordered Mesoporous Cr_2O_3. *Inorg. Chem.* **2012**, *51*, 11745−11752.
(40) Grewe, T.; Deng, X.; Weidenthaler, C.; Schüth, F.; Tüysüz, H. Design of Ordered Mesoporous Composite Materials and Their Electrocatalytic Activities for Water Oxidation. *Chem. Mater.* **2013**, *25*, 4926−4935.
(41) Ren, Y.; Ma, Z.; Morris, R. E.; Liu, Z.; Jiao, F.; Dai, S.; Bruce, P. G. A Solid with a Hierarchical Tetramodal Micro-Meso-Macro Pore Size Distribution. *Nat. Commun.* **2013**, *4*, 2015.
(42) Walcarius, A. Mesoporous Materials and Electrochemistry. *Chem. Soc. Rev.* **2013**, *42*, 4098−4140.
(43) Nakayama, S.; Kimura, A.; Shibata, M.; Kuwabata, S.; Osakai, T. Voltammetric Characterization of Oxide Films Formed on Copper in Air. *J. Electrochem. Soc.* **2001**, *148*, B467−B472.
(44) Kang, M.; Gewirth, A. A. Voltammetric and Force Spectroscopic Examination of Oxide Formation on Cu(111) in Basic Solution. *J. Phys. Chem. B* **2002**, *106*, 12211−12220.
(45) Liu, M. C.; Kong, L. B.; Lu, C.; Ma, X. J.; Li, X. M.; Luo, Y. C.; Kang, L. Design and Synthesis of $CoMoO_4$-$NiMoO_4$·xH_2O Bundles with Improved Electrochemical Properties for Supercapacitors. *J. Mater. Chem. A* **2013**, *1*, 1380−1387.
(46) Yuan, C.; Zhang, X.; Su, L.; Gao, B.; Shen, L. Facile Synthesis and Self-Assembly of Hierarchical Porous NiO Nano/micro Spherical Superstructures for High Performance Supercapacitors. *J. Mater. Chem. A* **2009**, *19*, 5772−5777.
(47) Yuan, C.; Yang, L.; Hou, L.; Shen, L.; Zhang, X.; Lou, X. W. Growth of Ultrathin Mesoporous Co_3O_4 Nanosheet Arrays on Ni Foam for High-Performance Electrochemical Capacitors. *Energy Environ. Sci.* **2012**, *5*, 7883−7887.
(48) Yuan, C.; Li, J.; Hou, L.; Zhang, X.; Shen, L.; Lou, X. W. Ultrathin Mesoporous $NiCo_2O_4$ Nanosheets Supported on Ni Foam as Advanced Electrodes for Supercapacitors. *Adv. Funct. Mater.* **2012**, *22*, 4592−4597.
(49) Ghenaatian, H. R.; Mousavi, M. F.; Rahmanifar, M. S. High Performance Hybrid Supercapacitor Based on Two Nanostructured Conducting Polymers: Self-Doped Polyaniline and Polypyrrole Nanofibers. *Electrochim. Acta* **2012**, *78*, 212−222.
(50) Li, Q.; Lu, X. F.; Xu, H.; Tong, Y. X.; Li, G. R. Carbon/MnO_2 Double-Walled Nanotube Arrays with Fast Ion and Electron Transmission for High-Performance Supercapacitors. *ACS Appl. Mater. Interfaces* **2014**, *6*, 2726−2733.
(51) Pendashteh, A.; Rahmanifar, M. S.; Kaner, R. B.; Mousavi, M. F. Facile Synthesis of Nanostructured $CuCo_2O_4$ as a Novel Electrode Material for High-Rate Supercapacitors. *Chem. Commun.* **2014**, *50*, 1972−1975.
(52) Guan, C.; Liu, J.; Cheng, C.; Li, H.; Li, X.; Zhou, W.; Zhang, H.; Fan, H. J. Hybrid Structure of Cobalt Monoxide Nanowire@Nickel Hydroxidenitrate Nanoflake Aligned on Nickel Foam for High-Rate Supercapacitor. *Energy Environ. Sci.* **2011**, *4*, 4496−4499.
(53) Bai, M. H.; Bian, L. J.; Song, Y.; Liu, X. X. Electrochemical Codeposition of Vanadium Oxide and Polypyrrole for High-Performance Supercapacitor with High Working Voltage. *ACS Appl. Mater. Interfaces* **2014**, *6*, 12656−12664.
(54) Yuan, C.; Zhang, L.; Hou, L.; Pang, G.; Oh, W.-C. One-Step Hydrothermal Fabrication of Strongly Coupled Co_3O_4 Nanosheets-Reduced Graphene Oxide for Electrochemical Capacitors. *RSC Adv.* **2014**, *4*, 14408−14413.
(55) Lu, X. F.; Wu, D. J.; Li, R. Z.; Li, Q.; Ye, S. H.; Tong, Y. X.; Li, G. R. Hierarchical $NiCo_2O_4$ Nanosheets@Hollow Microrod Arrays for High-Performance Asymmetric Supercapacitors. *J. Mater. Chem. A* **2014**, *2*, 4706−4713.
(56) Luan, F.; Wang, G.; Ling, Y.; Lu, X.; Wang, H.; Tong, Y.; Liu, X. X.; Li, Y. High Energy Density Asymmetric Supercapacitors with a Nickel Oxide Nanoflake Cathode and a 3D Reduced Graphene Oxide Anode. *Nanoscale* **2013**, *5*, 7984−7990.
(57) Yu, W.; Lin, W.; Shao, X.; Hu, Z.; Li, R.; Yuan, D. High Performance Supercapacitor Based on Ni_3S_2/Carbon Nanofibers and Carbon Nanofibers Electrodes Derived from Bacterial Cellulose. *J. Power Sources* **2014**, *272*, 137−143.
(58) Jing, M.; Yang, Y.; Zhu, Y.; Hou, H.; Wu, Z.; Ji, X. An Asymmetric Ultracapacitors Utilizing α-$Co(OH)_2$/Co_3O_4 Flakes Assisted by Electrochemically Alternating Voltage. *Electrochim. Acta* **2014**, *141*, 234−240.

DOI: 10.1021/am508816t
ACS Appl. Mater. Interfaces 2015, 7, 4851−4860

(59) El-Kady, M. F.; Kaner, R. B. Scalable Fabrication of High-Power Graphene Micro-Supercapacitors for Flexible and on-Chip Energy Storage. *Nat. Commun.* **2013**, *4*, 1475.
(60) El-Kady, M. F.; Strong, V.; Dubin, S.; Kaner, R. B. Laser Scribing of High-Performance and Flexible Graphene-Based Electrochemical Capacitors. *Science* **2012**, *335*, 1326−1330.
(61) Zhang, J.; Jiang, J.; Li, H.; Zhao, X. S. A High-Performance Asymmetric Supercapacitor Fabricated with Graphene-Based Electrodes. *Energy Environ. Sci.* **2011**, *4*, 4009−4015.
(62) He, Y.; Chen, W.; Li, X.; Zhang, Z.; Fu, J.; Zhao, C.; Xie, E. Freestanding Three-Dimensional Graphene/MnO_2 Composite Networks as Ultralight and Flexible Supercapacitor Electrodes. *ACS Nano* **2013**, *7*, 174−182.
(63) Fan, Z.; Yan, J.; Wei, T.; Zhi, L.; Ning, G.; Li, T.; Wei, F. Asymmetric Supercapacitors Based on Graphene/MnO_2 and Activated Carbon Nanofiber Electrodes with High Power and Energy Density. *Adv. Funct. Mater.* **2011**, *21*, 2366−2375.
(64) Yu, C.; Masarapu, C.; Rong, J.; Wei, B.; Jiang, H. Stretchable Supercapacitors Based on Buckled Single-Walled Carbon-Nanotube Macrofilms. *Adv. Mater.* **2009**, *21*, 4793−4797.
(65) Qu, Q.; Zhu, Y.; Gao, X.; Wu, Y. Core−Shell Structure of Polypyrrole Grown on V_2O_5 Nanoribbon as High Performance Anode Material for Supercapacitors. *Adv. Energy Mater.* **2012**, *2*, 950−955.
(66) Wang, D. W.; Li, F.; Cheng, H. M. Hierarchical Porous Nickel Oxide and Carbon as Electrode Materials for Asymmetric Supercapacitor. *J. Power Sources* **2008**, *185*, 1563−1568.
(67) Lei, Z.; Zhang, J.; Zhao, X. S. Ultrathin MnO_2 Nanofibers Grown on Graphitic Carbon Spheres as High-Performance Asymmetric Supercapacitor Electrodes. *J. Mater. Chem. A* **2012**, *22*, 153−160.
(68) Tang, C.; Tang, Z.; Gong, H. Hierarchically Porous Ni−Co Oxide for High Reversibility Asymmetric Full-Cell Supercapacitors. *J. Electrochem. Soc.* **2012**, *159*, A651−A656.
(69) Tang, Y.; Liu, Y.; Yu, S.; Mu, S.; Xiao, S.; Zhao, Y.; Gao, F. Morphology Controlled Synthesis of Monodisperse Cobalt Hydroxide for Supercapacitor with High Performance and Long Cycle Life. *J. Power Sources* **2014**, *256*, 160−169.
(70) Huang, M.; Zhang, Y.; Li, F.; Zhang, L.; Wen, Z.; Liu, Q. Facile Synthesis of Hierarchical Co_3O_4@MnO_2 Core−Shell Arrays on Ni Foam for Asymmetric Supercapacitors. *J. Power Sources* **2014**, *252*, 98−106.

DOI: 10.1021/am508816t
ACS Appl. Mater. Interfaces 2015, 7, 4851−4860